Vis Comput (2012) 28:573–583
DOI 10.1007/s00371-012-0693-0

ORIGINAL ARTICLE

Controllable C1 continuous blending of time-dependent parametric surfaces

L.H. You · H. Ugail · Jian J. Zhang

Published online: 18 April 2012

Abstract This paper proposes the concept of blending time-dependent varying surfaces, and develops a new method to create a controllable C1 continuous blending surface between primary parametric surfaces whose position and shape change with time. We treat it as a boundary-valued problem defined by the mathematical model of a vectored dynamic fourth-order partial differential equation subjected to time-dependent C1 continuous blending boundary constraints. High performance blending surface generation is achieved through the development of an approximate analytical solution of the mathematical model. We investigate the accuracy and efficiency of the solution, study the effective shape control of the blending surfaces, and apply the obtained solution to tackle surface blending problems. The applications demonstrate that our proposed approach is very effective and efficient in dealing with controllable C1 continuous surface blending between time-dependent varying parametric surfaces.

Keywords Surface blending · Varying parametric surfaces · C1 continuity · Dynamic partial differential equations · Approximate analytical solution · Shape control

L.H. You (✉) · J.J. Zhang
National Center for Computer Animation, Bournemouth University, Bournemouth, UK
e-mail: lyou@bournemouth.ac.uk

J.J. Zhang
e-mail: jzhang@bournemouth.ac.uk

H. Ugail
Center for Visual Computing, University of Bradford, Bradford, UK
e-mail: h.ugail@bradford.ac.uk

1 Introduction

Surface blending has a wide range of applications in computer graphics, computer animation, computer aided design, and manufacturing. Various blending methods have been developed in the existing literature.

According to a comprehensive survey made by Vida et al. [1], existing surface blending methods can be classified into five categories which are: rolling-ball blends, spine-based blends, trimline-based blends, polyhedral methods, and other methods including use of partial differential equations and Fourier-based approach.

All the above blending methods are applicable only to static surface blending, i. e., both the blending surface and the primary surfaces do not change with time. However, in nature and engineering applications, the shape of many primary surfaces usually changes with time. For example, the transition parts between the limbs and torso of animals including humans change their shapes when walking or running. How to blend varying surfaces of limbs and torso is an interesting topic in the field of computer graphics. Even in the field of computer aided design, we also face time-dependent surface blending problems. Surfaces under load conditions will deform causing a time-dependent stress change. Existing blending methods only consider how to generate a blending surface between unchangeable surfaces, but fail to consider how to achieve an optimal dynamic blending surface such that the stress change can be minimized. This is especially important for the applications requiring light weight and high reliability, such as aircrafts.

In order to address this issue, we present a new concept of blending time-dependent varying surfaces. Since the acceleration and velocity affect the shape of a moving surface, surface blending between varying primary surfaces involves

dynamic shape changes. In addition, to have C1 continuity, the exact satisfaction of the blending boundary constraints and the shape control have to be achieved at the same time, i.e. to resolve a boundary constrained problem where the dynamic shape change of blending surfaces is controllable. We present a mathematical model to deal with such a problem. To enable real-time engineering applications, we develop an efficient and effective solution to the mathematical model which can create blending surfaces quickly.

The contributions are: (1) initiating the research into time-dependent dynamic surface blending, (2) formulating a mathematical model of boundary constrained dynamic surface blending, (3) developing an efficient and effective solution of the mathematical model, and (4) solving the problem of controllable C1 continuous blending surfaces between varying parametric surfaces.

In what follows, we first review the related work in Sect. 2. Then we formulate the blending boundary constraints and mathematical model of controllable dynamic surface blending, and develop an efficient and effective solution in Sect. 3. Next, we investigate the accuracy and efficiency of the proposed solution, and discuss shape control of blending surfaces in Sect. 4. Following that, we give some examples of blending time-dependent varying parametric surfaces in Sect. 5. The work is concluded in Sect. 6.

2 Related work

Surface blending is to smoothly connect separate surfaces together. The surfaces to be connected are called primary or base surfaces. The surface which connects primary surfaces is called a blending surface. The interfaces between blending and primary surfaces are called trimlines.

Various surface blending methods have been reviewed by Vida et al. [1]. Here we introduce rolling-ball methods and PDE-based modeling approaches.

Rolling-ball methods are very popular in surface blending. They can be used to blend both implicit and parametric surfaces. This method creates a blending surface by rolling a ball along two primary surfaces. It was first proposed by Rossignac and Requicha [2]. Later on, Choi and Ju proposed a blending method which achieves rolling-ball (edge) blends and corner blends by sweeping rational quadratic (conic section) curves and through a convex combination of linear Taylor interpolants, respectively [3]. Sanglikar et al. developed a mathematical model of rolling-ball blending, and provided closed-form analytical solutions for most of the surfaces which are common in current solid modelers [4]. Based on finding the intersection of two offset surfaces using only the first-order derivatives of the progenitors, Barnhill et al. presented a method for blending two parametric surfaces [5]. Chuang et al. computed a parametric form of the variable-radius spherical and circular blends with the derived spine curve and linkage curves [6]. By tracing the intersection of the offsets to the given surfaces and corresponding normal projection curves on those surfaces with a pseudo-arclength predictor-corrector scheme, Farouki and Sverrisson used numerical methods to create constant-radius blends between intersecting parametric surfaces with prescribed-precision approximation [7]. Since the radius of variable-radius blending is hard to specify and the spine curve is hard to trace, Chuang and Hwang proposed several geometric constraints to specify the variable radius [8]. Chuang and Lien investigated an exact formulation and a flexible one. The former represents the blend as the swept surface of the intersection between the offsets of the primary surfaces whose radii satisfy specific one-parametric curve. And the latter also defines the blend as a swept surface but its radii satisfy a specific two-parameter surface [9]. Lukács studied the differential geometry of G^1 variable-radius rolling-ball blending surfaces with an implicit representation [10]. Kós et al. presented and compared various algorithms for recovering constant-radius rolling-ball blends [11].

In spite of the popularity of rolling-ball methods, they can create G1 continuous blends only. In contrast, the partial differential equation based method can create C1 continuous blending surfaces between separate parametric surfaces. This method uses the solution to a vector-valued partial differential equation subjected to blending boundary constraints to create blending surfaces. It was first proposed by Bloor and Wilson [12]. Since partial differential equations are difficult to solve, various approximate analytical and numerical methods were created. Cheng et al. presented a finite difference method to construct blending surfaces between quadric surfaces [13]. Bloor and Wilson derived a method of collocation by using B-splines [14]. They also employed Fourier series method to generate free-form surfaces [15]. By introducing a remainder function into a Fourier series, they proposed a spectral method to solve a vector-valued partial differential equation (PDE) and generate PDE surfaces [16]. Later on, they investigated a perturbation method to tackle partial differential equation based surface blending problems [17]. Brown et al. determined the accuracy using B-spline finite element to approximate PDE surfaces [18]. Li examined the basic theory of boundary penalty finite element methods as well as superconvergence and stability [19–21]. You et al. investigated C1 continuous surface blending [22], and C2 continuous blending surfaces [23].

Apart from the applications in surface blending, partial differential equations have also been applied in interactive surface design [24], free-form surface modeling [25], cyclic animation [26], patchwise approximation of large polygon meshes [27], and solid modeling [28].

The proposed approach is related to but different from the existing PDE-based modeling approaches. It proposes PDE-based dynamic surface blending between time-dependent varying parametric surfaces.

3 Mathematical model and solution

In order to achieve a smooth transition between blending and primary surfaces, tangent continuity at the interfaces is usually required. For some special applications requiring better smoothness, such as the design of streamlined surfaces of aircraft, ships and cars, curvature continuity has to be introduced.

Tangent continuity can be divided into G1 and C1 continuities which are called geometric or parametric continuities, respectively. If the directions of tangent vectors of primary and blending surfaces at trimlines are the same but the magnitudes of the tangent vectors are different, G1 continuity is achieved. If both the directions and magnitudes of the tangent vectors of primary and blending surfaces at trimlines are equal, C1 continuity is reached. In this paper, we aim to develop C1 continuous blending approach between varying surfaces.

If the first partial derivatives of primary and blending surfaces at trimlines are identical, the directions and magnitudes of tangent vectors of primary and blending surfaces at trimlines are also equal. Therefore, we obtain C1 continuity by taking the first partial derivatives of the blending surface at trimlines to be those of primary surfaces at the same positions.

Two time-dependent varying primary parametric surfaces to be blended together can be represented with the mathematical equations $\mathbf{S}_1(u,v,t)$ and $\mathbf{S}_2(u,v,t)$, where u and v are two parametric variables, t is a time variable, and $\mathbf{S}_i(u,v,t) = [S_{xi}(u,v,t)\ S_{yi}(u,v,t)\ S_{zi}(u,v,t)]^T$ $(i = 1, 2)$ are vector-valued functions. If the two surfaces will be connected together at the positions u_1 and u_2, the position function and the first partial derivative determined by the first primary parametric surface $\mathbf{S}_1(u,v,t)$ are $\mathbf{S}_1(u_1,v,t)$ and $\partial\mathbf{S}_1(u_1,v,t)/\partial u$, and those determined by the second primary parametric surface $\mathbf{S}_2(u,v,t)$ are $\mathbf{S}_2(u_2,v,t)$ and $\partial\mathbf{S}_2(u_2,v,t)/\partial u$. Assuming that the vector-valued mathematical equation of the blending surface is $\mathbf{S}(u,v,t)$, it is connected to the first primary parametric surface at the position $u = 0$ and the second primary parametric surface at the position $u = 1$. In order to achieve C1 continuity, the position functions and the first partial derivatives of the blending surface at these positions should be exactly the same as those of primary parametric surfaces. If we introduce $\mathbf{C}_0(v,t)$, $\mathbf{T}_0(v,t)$, $\mathbf{C}_1(v,t)$ and $\mathbf{T}_1(v,t)$ with

$$\begin{aligned}
&\mathbf{C}_0(v,t) = \mathbf{S}_1(u_1,v,t),\\
&\mathbf{T}_0(v,t) = \partial\mathbf{S}_1(u_1,v,t)/\partial u,\\
&\mathbf{C}_1(v,t) = \mathbf{S}_2(u_2,v,t),\\
&\mathbf{T}_1(v,t) = \partial\mathbf{S}_2(u_2,v,t)/\partial u,
\end{aligned} \tag{1}$$

the following blending boundary constraints are obtained:

$$\begin{aligned}
&u = 0,\\
&\mathbf{S}(u,v,t) = \mathbf{C}_0(v,t), \qquad \partial\mathbf{S}(u,v,t)/\partial u = \mathbf{T}_0(v,t),\\
&u = 1,\\
&\mathbf{S}(u,v,t) = \mathbf{C}_1(v,t), \qquad \partial\mathbf{S}(u,v,t)/\partial u = \mathbf{T}_1(v,t),
\end{aligned} \tag{2}$$

where

$$\mathbf{C}_i(v,t) = \left[C_{xi}(v,t)\ C_{yi}(v,t)\ C_{zi}(v,t)\right]^T, \quad \text{and}$$
$$\mathbf{T}_i(v,t) = \left[T_{xi}(v,t)\ T_{yi}(v,t)\ T_{zi}(v,t)\right]^T \quad (i = 0, 1).$$

When the position and shape of the primary parametric surfaces vary with time, the blending surface between the primary parametric surfaces changes its position and shape accordingly, and the change is also affected by the velocity and acceleration of the blending surface in motion. Surface blending between varying primary surfaces should consider such dynamic shape changes. In addition, it is required in many applications that the blending surface not only satisfies blending boundary constraints exactly but also meets some functionalities such as an acceptable or pleasing shape or a uniform stress distribution in the blending surface. Controllable shape changes of blending surfaces can satisfy such functionalities.

From the above discussions, we can conclude that the surface blending between varying primary surfaces can be treated as boundary constrained dynamic shape changes of controllable blending surfaces. It can be formulated as a mathematical boundary-value problem defined by the following mathematical model (3) subjected to blending boundary constraints (2):

$$\left(\beta\frac{\partial^4}{\partial u^4} + \gamma\frac{\partial^4}{\partial u^2\partial v^2} + \lambda\frac{\partial^4}{\partial v^4} + \rho\frac{\partial^2}{\partial t^2} + \eta\frac{\partial}{\partial t}\right)\mathbf{S}(u,v,t) = \mathbf{q}, \tag{3}$$

where β, γ, λ, ρ, and η are shape control parameters which can be used to control the shape of blending surfaces effectively. Parameters ρ and η are also called density and viscous damping coefficients whose combinations with ac-

celeration and velocity describe dynamic effects, i.e., the effects of acceleration and velocity on shape changes of blending surfaces. And $\mathbf{q}$ is a vector-valued force function which also has a great influence on shape changes of the blending surface. We will investigate it in our following work. In this paper, we will not consider the force function for sake of simplifying the solution of Eq. (3) which is a vector-valued fourth-order PDE.

The complexity of solving PDE (3) is determined by blending boundary constraints (2). For some simple cases, the exact analytical solution of PDE (3) is obtainable. For example, when all the functions in blending boundary constraints are constants, we can always construct a polynomial of variables u, v and t so that both blending boundary constraints (2) and PDE (3) can be exactly satisfied. However, for general cases, the exact analytical solution of PDE (3) is not obtainable and an approximate analytical solution has to be found to create time-dependent varying blending surfaces quickly. We will develop such an approximate analytical solution below.

The above discussion indicates that the construction of the approximate analytical solution to PDE (3) should consider blending boundary constraints. Since blending boundary constraints are the functions of parametric variable v and time variable t, these functions can be written as $F_j(v,t)$ $(j=1,2,\ldots,J)$. Therefore, the vector-valued mathematical equation of blending surfaces can be defined as a combination of $F_j(v,t)$ with some unknown functions $\mathbf{G}_j(u)$, i.e.,

$$\mathbf{S}(u,v,t)=\sum_{j=1}^{J}\mathbf{G}_j(u)F_j(v,t). \tag{4}$$

Substituting Eq. (4) into PDE (3), we obtain the following equation:

$$\begin{aligned}\sum_{j=1}^{J}\Bigg\{&\beta\frac{\partial^4\mathbf{G}_j(u)}{\partial u^4}F_j(v,t)+\gamma\frac{\partial^2\mathbf{G}_j(u)}{\partial u^2}\frac{\partial^2F_j(v,t)}{\partial v^2}\\&+\lambda\mathbf{G}_j(u)\frac{\partial^4F_j(v,t)}{\partial v^4}\\&+\mathbf{G}_j(u)\left[\rho\frac{\partial^2F_j(v,t)}{\partial t^2}+\eta\frac{\partial F_j(v,t)}{\partial t}\right]\Bigg\}=\mathbf{q}.\end{aligned} \tag{5}$$

Since all the functions in blending boundary constraints (2) can be formulated as $F_j(v,t)$ $(j=1,2,\ldots,J)$, blending boundary constraints can be transformed into

$$\begin{aligned}&u=0,\quad \mathbf{S}(u,v,t)=\sum_{j=1}^{J}\mathbf{b}_jF_j(v,t),\\&\frac{\partial\mathbf{S}(u,v,t)}{\partial u}=\sum_{j=1}^{J}\bar{\mathbf{b}}_jF_j(v,t),\\&u=1,\quad \mathbf{S}(u,v,t)=\sum_{j=1}^{J}\mathbf{d}_jF_j(v,t),\\&\frac{\partial\mathbf{S}(u,v,t)}{\partial u}=\sum_{j=1}^{J}\bar{\mathbf{d}}_jF_j(v,t),\end{aligned} \tag{6}$$

where $\mathbf{b}_j=[b_{xj}\ b_{yj}\ b_{zj}]^T$, $\bar{\mathbf{b}}_j=[\bar{b}_{xj}\ \bar{b}_{yj}\ \bar{b}_{zj}]^T$, $\mathbf{d}_j=[d_{xj}\ d_{yj}\ d_{zj}]^T$ and $\bar{\mathbf{d}}_j=[\bar{d}_{xj}\ \bar{d}_{yj}\ \bar{d}_{zj}]^T$ $(j=1,2,\ldots,J)$ are known vector-valued constants.

For example, if in blending boundary constraints (2) we have: $C_{0x}(v,t)=a_{11}t\sin v$, $C_{0y}(v,t)=a_{12}t\cos v$, $C_{0z}(v,t)=a_{13}t$, $T_{0x}(v,t)=a_{21}$, $T_{0y}(v,t)=a_{22}v$, $T_{0z}(v,t)=a_{23}t$, $C_{1x}(v,t)=a_{31}v$, $C_{1y}(v,t)=a_{32}v^2$, $C_{1z}(v,t)=a_{33}$, $T_{1x}(v,t)=a_{41}vt$, $T_{1y}(v,t)=a_{42}e^v$ and $T_{1z}(v,t)=a_{43}$, the functions in blending boundary constraints (6) are: $F_1(v,t)=1$, $F_2(v,t)=t$, $F_3(v,t)=v$, $F_4(v,t)=v^2$, $F_5(v,t)=e^v$, $F_6(v,t)=t\sin v$, $F_7(v,t)=t\cos v$ and $F_8(v,t)=vt$. According to these functions and blending boundary constraints (6), we have $b_{x6}=a_{11}$, $b_{y7}=a_{12}$, $b_{z2}=a_{13}$, $\bar{b}_{x1}=a_{21}$, $\bar{b}_{y3}=a_{22}$, $\bar{b}_{z2}=a_{23}$, $d_{x3}=a_{31}$, $d_{y4}=a_{32}$, $d_{z1}=a_{33}$, $\bar{d}_{x8}=a_{41}$, $\bar{d}_{y5}=a_{42}$, $\bar{d}_{z1}=a_{43}$, and all other elements of $\mathbf{b}_j$, $\bar{\mathbf{b}}_j$, $\mathbf{d}_j$ and $\bar{\mathbf{d}}_j$ are zero.

Since $F_j(v,t)$ $(j=1,2,\ldots,J)$ are known functions, Eq. (5) is a vector-valued ordinary differential equation of parametric variable u. If the force function $\mathbf{q}$ is not considered, solving PDE (3) subjected to blending boundary constraints (2) can be transformed into solving a series of vector-valued ordinary differential equation of parametric variable u:

$$\begin{aligned}&\beta\frac{\partial^4\mathbf{G}_j(u)}{\partial u^4}F_j(v,t)+\gamma\frac{\partial^2\mathbf{G}_j(u)}{\partial u^2}\frac{\partial^2F_j(v,t)}{\partial v^2}+\mathbf{G}_j(u)\\&\left[\lambda\frac{\partial^4F_j(v,t)}{\partial v^4}+\rho\frac{\partial^2F_j(v,t)}{\partial t^2}+\eta\frac{\partial F_j(v,t)}{\partial t}\right]=0\end{aligned} \tag{7}$$

subjected to the following boundary constraints:

$$\begin{aligned}&u=0,\quad \mathbf{G}_j(u)=\mathbf{b}_j,\ \frac{d\mathbf{G}_j(u)}{du}=\bar{\mathbf{b}}_j,\\&u=1,\quad \mathbf{G}_j(u)=\mathbf{d}_j,\ \frac{d\mathbf{G}_j(u)}{du}=\bar{\mathbf{d}}_j,\end{aligned} \tag{8}$$

where $j=1,2,\ldots,J$.

Now we construct the vector-valued function $\mathbf{G}_j(u)$. The basic idea is to introduce a new function of parametric variable u which is the sum of a cubic polynomial and a sine

series. The cubic polynomial is used to exactly satisfy blending boundary constraints and the sine series is employed to minimize the error of PDE (3). Based on this consideration, the vector-valued function $\mathbf{G}_j(u)$ is taken to be

$$\mathbf{G}_j(u) = \sum_{k=0}^{3} \mathbf{c}_{jk} u^k + \sum_{k=1}^{K} \mathbf{P}_{jk} \sin k\pi u, \tag{9}$$

where $\mathbf{c}_{jk} = [c_{xjk}\ c_{yjk}\ c_{zjk}]^T$ $(j = 1, 2, \ldots, J; k = 0, 1, 2, 3)$ and $\mathbf{P}_{jk} = [P_{xjk}\ P_{yjk}\ P_{zjk}]^T$ $(j = 1, 2, \ldots, J;\ k = 1, 2, \ldots, K)$ are vector-valued unknown constants, and K is the total term of the sine series.

Substituting the vector-valued function $\mathbf{G}_j(u)$ and its first derivative with respect to parametric variable u into boundary constraints (8), solving for the vector-valued unknown constants $\mathbf{c}_{j0}$, $\mathbf{c}_{j1}$, $\mathbf{c}_{j2}$ and $\mathbf{c}_{j3}$, we obtain

$$\begin{aligned}
\mathbf{c}_{j0} &= \mathbf{b}_j, \\
\mathbf{c}_{j1} &= \bar{\mathbf{b}}_j, \\
\mathbf{c}_{j2} &= -3\mathbf{b}_j - 2\bar{\mathbf{b}}_j + 3\mathbf{d}_j - \bar{\mathbf{d}}_j + \pi \sum_{k=1}^{K} (-1)^k k \mathbf{P}_{jk}, \\
\mathbf{c}_{j3} &= 2\mathbf{b}_j + \bar{\mathbf{b}}_j - 2\mathbf{d}_j + \bar{\mathbf{d}}_j - \pi \sum_{k=1}^{K} (-1)^k k \mathbf{P}_{jk}.
\end{aligned} \tag{10}$$

Substituting $\mathbf{c}_{j0}$, $\mathbf{c}_{j1}$, $\mathbf{c}_{j2}$ and $\mathbf{c}_{j3}$ back to Eq. (9), we obtain the following vector-valued function $\mathbf{G}_j(u)$ which has satisfied blending boundary constraints (8) exactly:

$$\begin{aligned}
\mathbf{G}_j(u) = {} & \xi_1(u)\mathbf{b}_j + \xi_2(u)\bar{\mathbf{b}}_j + \xi_3(u)\mathbf{d}_j + \xi_4(u)\bar{\mathbf{d}}_j \\
& + \sum_{k=1}^{K} \varsigma(u, k)\mathbf{P}_{jk},
\end{aligned} \tag{11}$$

where

$$\begin{aligned}
\xi_1(u) &= 1 - (3 - 2u)u^2, \\
\xi_2(u) &= \big[1 - (2 - u)u\big]u, \\
\xi_3(u) &= (3 - 2u)u^2, \\
\xi_4(u) &= (-1 + u)u^2, \\
\varsigma(u, k) &= (-1)^k k\pi(1 - u)u^2 + \sin k\pi u.
\end{aligned} \tag{12}$$

Next, we make the vector-valued function $\mathbf{G}_j(u)$ best approximate Eq. (7) by using the least squared approximation to minimize the error of Eq. (7).

First, we substitute Eq. (11) and its second and fourth derivatives into Eq. (7), and obtain an error function of the equation. Then, we collocate $L \times M$ points in the region where the blending surface is defined, and calculate the squared sum of the error function at these points with

$$\mathbf{E} = \sum_{l=1}^{L} \sum_{m=1}^{M} \left[\sum_{k=1}^{K} \varphi_1(u_l, v_m, t, j, k)\mathbf{P}_{jk} + \varphi_2(u_l, v_m, t, j) \right]^2, \tag{13}$$

where

$$\begin{aligned}
&\varphi_1(u_l, v_m, t, j, k) \\
&\quad = \beta\pi^4 k^4 \sin k\pi u_l F_j(v_m, t) \\
&\qquad + \gamma\pi k\big[(-1)^k(2 - 6u_l) - \pi k \sin k\pi u\big]\partial^2 F_j(v_m, t)/\partial v^2 \\
&\qquad + \big[(-1)^k \pi k(1 - u_l)u_l^2 + \sin k\pi u\big]\big[\lambda\partial^4 F_j(v_m, t)/\partial v^4 \\
&\qquad + \rho\partial^2 F_j(v_m, t)/\partial t^2 + \eta\partial F_j(v_m, t)/\partial t\big]
\end{aligned} \tag{14}$$

and

$$\begin{aligned}
&\varphi_2(u_l, v_m, t, j) \\
&\quad = -2\gamma\big[3\mathbf{b}_j + 2\bar{\mathbf{b}}_j - 3\mathbf{d}_j + \bar{\mathbf{d}}_j \\
&\qquad + 3(4\mathbf{b}_j + 2\bar{\mathbf{b}}_j - 4\mathbf{d}_j + 2\bar{\mathbf{d}}_j)u_l\big]\partial^2 F_j(v_m, t)/\partial v^2 \\
&\qquad + \big[\mathbf{b}_j + \bar{\mathbf{b}}_j u_l - (3\mathbf{b}_j + 2\bar{\mathbf{b}}_j - 3\mathbf{d}_j + \bar{\mathbf{d}}_j)u_l^2 \\
&\qquad + (2\mathbf{b}_j + \bar{\mathbf{b}}_j - 2\mathbf{d}_j + \bar{\mathbf{d}}_j)u_l^3\big]\big[\lambda\partial^4 F_j(v_m, t)/\partial v^4 \\
&\qquad + \rho\partial^2 F_j(v_m, t)/\partial t^2 + \eta\partial F_j(v_m, t)/\partial t\big].
\end{aligned} \tag{15}$$

The squared error sum $\mathbf{E}$ can be minimized by zeroing the first partial derivative of the squared error sum $\mathbf{E}$ with respect to the vector-valued unknown constants $\mathbf{P}_{jr}$ $(r = 1, 2, 3, \ldots, K)$, i.e.,

$$\partial\mathbf{E}/\partial\mathbf{P}_{jr} = 0 \quad (r = 1, 2, 3, \ldots, K) \tag{16}$$

which gives

$$\begin{aligned}
&\sum_{l=1}^{L} \sum_{m=1}^{M} \left\{ \sum_{k=1}^{K} \varphi_1(u_l, v_m, t, j, k)\mathbf{P}_{jk} \right. \\
&\quad \left. + \varphi_2(u_l, v_m, t, j) \right\} \varphi_1(u_l, v_m, t, j, r) = 0. \\
&\quad (r = 1, 2, 3, \ldots, K)
\end{aligned} \tag{17}$$

There are K linear algebra equations in Eq. (17) which can be used to determine the K unknown constants $\mathbf{P}_{jk}$ $(k = 1, 2, 3, \ldots, K)$. Substituting $\mathbf{P}_{jk}$ back into Eq. (11), we obtain the vector-valued function $\mathbf{G}_j(u)$. Repeating the above process for $j = 1, 2, 3, \ldots, J$, we obtain all the vector-valued functions $\mathbf{G}_j(u)$ $(j = 1, 2, 3, \ldots, J)$. Substituting all these vector-valued functions, i.e., Eq. (11) into Eq. (4), the vector-valued mathematical equation of blending surfaces is

found to be

$$\mathbf{S}(u,v,t)=\sum_{j=1}^{J}\Bigg[\xi_1(u)\mathbf{b}_j+\xi_2(u)\bar{\mathbf{b}}_j+\xi_3(u)\mathbf{d}_j+\xi_4(u)\bar{\mathbf{d}}_j+\sum_{k=1}^{K}\varsigma(u,k)\mathbf{P}_{jk}\Bigg]F_j(v,t). \tag{18}$$

We have implemented the above approach using OpenGL. The developed software is applicable to all surface blending problems between two separate primary parametric surfaces. It can automatically construct C1 continuous blending surfaces after inputting all the shape control parameters, functions $F_j(v,t)$ $(j=1,2,\ldots,J)$, vector-valued constants $\mathbf{b}_j$, $\bar{\mathbf{b}}_j$, $\mathbf{d}_j$ and $\bar{\mathbf{d}}_j$ $(j=1,2,3,\ldots,J)$ and the values of L and M into Eq. (13). It can be also used to manipulate the shape of blending surfaces interactively.

In the following sections, we will investigate the accuracy and efficiency of the obtained approximate analytical solution, discuss shape control of blending surfaces, and present two examples to demonstrate the applications of Eq. (18) in dynamic surface blending between time-dependent varying parametric surfaces.

4 Accuracy, efficiency and shape control

In this section, we investigate the computational accuracy, efficiency, and shape control of blending surfaces. For the evaluation of computational accuracy and efficiency of the proposed approach, the best method is to compare the solution of the proposed approach with the corresponding closed-form analytical solution which is the most accurate and efficient.

In order to obtain such a closed-form analytical solution, we design the following blending boundary constraints:

$$\begin{aligned}
&u=0,\\
&S_x=ae^t\sin v,\qquad S_y=be^{-t}\cos v,\qquad S_z=h_0\\
&\frac{\partial S_x}{\partial u}=0,\qquad \frac{\partial S_y}{\partial u}=0,\qquad \frac{\partial S_z}{\partial u}=h_1\\
&u=1,\\
&S_x=ce^{-t}\sin v,\qquad S_y=de^{t}\cos v,\qquad S_z=0\\
&\frac{\partial S_x}{\partial u}=0,\qquad \frac{\partial S_y}{\partial u}=0,\qquad \frac{\partial S_z}{\partial u}=h_1
\end{aligned} \tag{19}$$

where a, b, c, d, h_0 and h_1 are known constants.

The above blending boundary constraints are from two elliptic cylinders. When the time variable increases from 0 to 0.3, both elliptic cylinders change from one shape to other shapes continuously.

From blending boundary constraints (19), we know that the functions $F_j(v,t)$ are: $F_1(v,t)=e^t\sin v$, $F_2(v,t)=e^{-t}\sin v$, $F_3(v,t)=e^t\cos v$, $F_4(v,t)=e^{-t}\cos v$, and $F_5(v,t)=1$. Therefore, the vector-valued mathematical equation of the blending surface should be

$$\mathbf{S}(u,v,t)=\mathbf{G}_1(u)e^t\sin v+\mathbf{G}_2(u)e^{-t}\sin v+\mathbf{G}_3(u)e^t\cos v+\mathbf{G}_4(u)e^{-t}\cos v+\mathbf{G}_5(u). \tag{20}$$

Substituting Eq. (20) into Eq. (3), the vector-valued partial differential equation is transformed into 5 vector-valued ordinary differential equations which will be given below. For the first and third terms on the right-hand side of Eq. (20), the vector-valued ordinary differential equations are

$$\beta\frac{d^4\mathbf{G}_j(u)}{du^4}-\gamma\frac{d^2\mathbf{G}_j(u)}{du^2}+(\lambda+\rho+\eta)\mathbf{G}_j(u)=0.\quad(j=1,3) \tag{21}$$

For the second and fourth terms on the right-hand side of Eq. (20), the vector-valued ordinary differential equations can be written as

$$\beta\frac{d^4\mathbf{G}_j(u)}{du^4}-\gamma\frac{d^2\mathbf{G}_j(u)}{du^2}+(\lambda+\rho-\eta)\mathbf{G}_j(u)=0.\quad(j=2,4) \tag{22}$$

For the fifth term on the right-hand side of Eq. (20), the vector-valued ordinary differential equation reads

$$\frac{d^4\mathbf{G}_5(u)}{du^4}=0. \tag{23}$$

For $\gamma^2>4\beta(\lambda+\rho+\eta)$ and $\gamma^2>4\beta(\lambda+\rho-\eta)$, the solution to Eqs. (21) and (22) has the form

$$\mathbf{G}_j(u)=\mathbf{f}_{j1}e^{q_1u}+\mathbf{f}_{j2}e^{q_2u}+\mathbf{f}_{j3}e^{q_3u}+\mathbf{f}_{j4}e^{q_4u}\quad(j=1,2,3,4) \tag{24}$$

where $\mathbf{f}_{j1}$, $\mathbf{f}_{j2}$, $\mathbf{f}_{j3}$ and $\mathbf{f}_{j4}$ $(j=1,2,3,4)$ are unknown vector-valued constants, $q_i=\bar{q}_i$ $(i=1,2,3,4)$ for Eq. (21), and $q_i=\hat{q}_i$ $(i=1,2,3,4)$ for Eq. (22).

For $\gamma^2>4\beta(\lambda+\rho+\eta)$,

$$\bar{q}_{1,2,3,4}=\pm\sqrt{\frac{\gamma\pm\sqrt{\gamma^2-4\beta(\lambda+\rho+\eta)}}{2\beta}}. \tag{25}$$

For $\gamma^2>4\beta(\lambda+\rho-\eta)$,

$$\hat{q}_{1,2,3,4}=\pm\sqrt{\frac{\gamma\pm\sqrt{\gamma^2-4\beta(\lambda+\rho-\eta)}}{2\beta}}. \tag{26}$$

The solution to the vector-valued ordinary differential equation (23) is

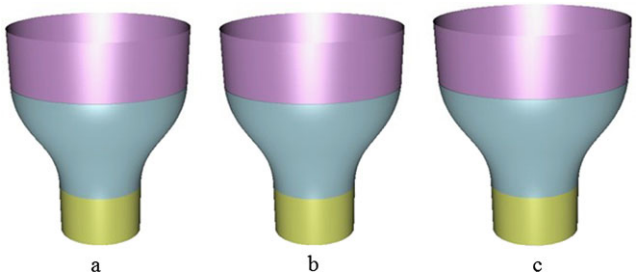

Fig. 1 Comparison between accurate and approximate solutions

$$\mathbf{G}_5(u) = \mathbf{f}_{51} + \mathbf{f}_{52}u + \mathbf{f}_{53}u^2 + \mathbf{f}_{54}u^3 \tag{27}$$

where $\mathbf{f}_{51}$, $\mathbf{f}_{52}$, $\mathbf{f}_{53}$ and $\mathbf{f}_{54}$ are unknown vector-valued constants.

Substituting Eqs. (24) and (27) into Eq. (20), we obtain the closed form solution:

$$\begin{aligned}\mathbf{S}(u,v,t) = {} & \left[\mathbf{f}_{11}e^{\bar{q}_1 u} + \mathbf{f}_{12}e^{\bar{q}_2 u} + \mathbf{f}_{13}e^{\bar{q}_3 u} + \mathbf{f}_{14}e^{\bar{q}_4 u}\right]e^{t}\sin v \\ & + \left[\mathbf{f}_{21}e^{\hat{q}_1 u} + \mathbf{f}_{22}e^{\hat{q}_2 u} + \mathbf{f}_{23}e^{\hat{q}_3 u} + \mathbf{f}_{24}e^{\hat{q}_4 u}\right] \\ & \times e^{-t}\sin v + \left[\mathbf{f}_{31}e^{\bar{q}_1 u} + \mathbf{f}_{32}e^{\bar{q}_2 u} + \mathbf{f}_{33}e^{\bar{q}_3 u}\right. \\ & \left. + \mathbf{f}_{34}e^{\bar{q}_4 u}\right]e^{t}\cos v + \left[\mathbf{f}_{41}e^{\hat{q}_1 u} + \mathbf{f}_{42}e^{\hat{q}_2 u}\right. \\ & \left. + \mathbf{f}_{43}e^{\hat{q}_3 u} + \mathbf{f}_{44}e^{\hat{q}_4 u}\right]e^{-t}\cos v \\ & + \mathbf{f}_{51} + \mathbf{f}_{52}u + \mathbf{f}_{53}u^2 + \mathbf{f}_{54}u^3. \end{aligned} \tag{28}$$

Substituting $\mathbf{S}(u, v, t)$ of Eq. (28) and its first partial derivatives with respect to parametric variable into blending boundary constraints (19), we determine all the unknown constants $\mathbf{f}_{j1}$, $\mathbf{f}_{j2}$, $\mathbf{f}_{j3}$ and $\mathbf{f}_{j4}$ $(j = 1, 2, 3, 4, 5)$. Inserting these unknown constants back into Eq. (28), the vector-valued closed-form solution of the blending surface is obtained.

Taking the known constants in Eq. (19) to be: $a = 1.6$, $b = 1$, $c = 0.8$, $d = 0.6$, $h_0 = 2$ and $h_1 = -3$, and shape control parameters to be: $\beta = \lambda = \rho = \eta = 1$ and $\gamma = 12.1$, the blending surface at the time $t = 0$ created by the closed-form solution (28) is depicted in Fig. 1(a). With the approximate analytical solution, 11×11 points are uniformly collocated in the region $\{0 \le u \le 1, 0 \le v \le 2\pi\}$, the blending surfaces at the time $t = 0$ from 5 and 7 terms of the sine series are shown in Fig. 1(b) and (c), respectively.

Comparing these images, we cannot find any visual differences even when the terms of the sine series are 5 only. It indicates that our proposed approximate analytical solution can produce very good approximate results.

On a laptop with 1.66-GHz CPU and creating the blending surface with 100×100 surface points, the used time is given in Table 1 where CFS stands for the closed-form solution, OPA indicates our proposed approach. Since the closed-form solution must calculate many terms of exponential and trigonometric functions, it took much more time to create the same blending surface than our proposed approximate analytical solution.

Table 1 Comparison of efficiency

Solution methods	CFS	OPA ($k = 5$)	OPA ($k = 10$)
Time (second)	0.597	0.077	0.111

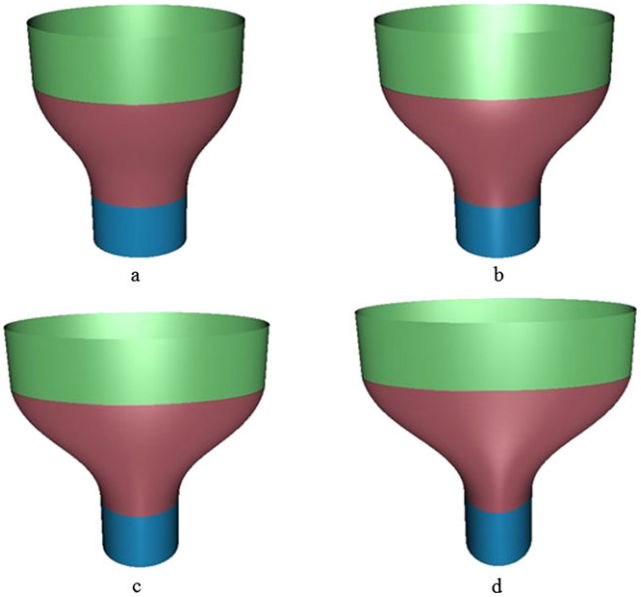

Fig. 2 Shape changes of primary and blending surfaces with time

When the time variable increases from $t = 0$, the top and bottom primary surfaces change their shapes continuously. The created blending surface always smoothly connects the two primary surfaces together as demonstrated in Fig. 2 where the shapes of the blending surface at $t = 0$, 0.1, 0.2 and 0.3 are depicted in parts (a)–(d) of the figure, respectively.

Now we discuss the shape control of blending surfaces. We will demonstrate below that each of the shape control parameters, including the density ρ and viscous damping coefficient η, can be used to control the shape of blending surfaces effectively.

In order to demonstrate the effect of the density ρ, we change the shape control parameters to: $\beta = \lambda = \eta = 0.01$ and $\gamma = 10$. When $\rho = 200$, the shape in part (a) of Fig. 3 is obtained. The shapes in parts (b) and (c) of the figure are from $\rho = 100$ and $\rho = 10$, respectively. These images show that increasing the density can make the blending surface more concave.

The influence of the viscous damping coefficient on the shape of blending surfaces is depicted in Fig. 4. The shape control parameters used to generate these images are: $\beta = \lambda = \rho = 0.01$ and $\gamma = 10$. When $\eta = -120$, the shape in part (a) of the figure is obtained. When η is changed to -100, the shape in part (b) is created. Further changing η

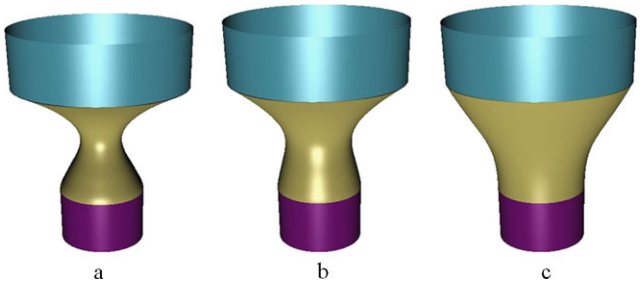

Fig. 3 Effect of the density on the shape of blending surfaces

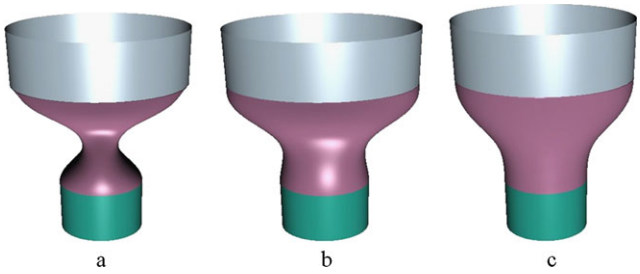

Fig. 4 Effect of the viscous damping coefficients on the shape of blending surfaces

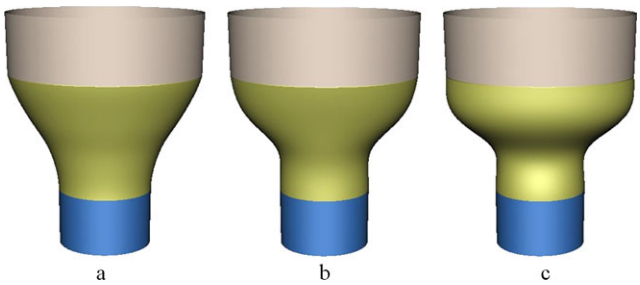

Fig. 5 Effect of the shape control parameter β on the shape of blending surfaces

to -50, the shape in part (c) is generated. These images indicate a strong effect of viscous damping coefficient on the shape of blending surfaces. As the viscous damping coefficient η changes from -120 to -50, the blending surface achieves better smoothness at both trimlines.

The effect of the shape control parameter β on the shape of blending surfaces is shown in Fig. 5. The shape control parameters are taken to be: $\lambda = \rho = 0.01$, $\gamma = 10$ and $\eta = -5$. The blending surfaces from $\beta = 0$, $\beta = -0.15$ and $\beta = -0.18$, are depicted in parts (a), (b) and (c) of the figure, respectively.

These images indicate that the shape control parameter β can greatly enhance the smoothness between primary parametric surfaces and the blending surface as well. As the shape control parameter β changes from 0 to -0.18, a smoother transition of the blending surface at the trimlines is achieved.

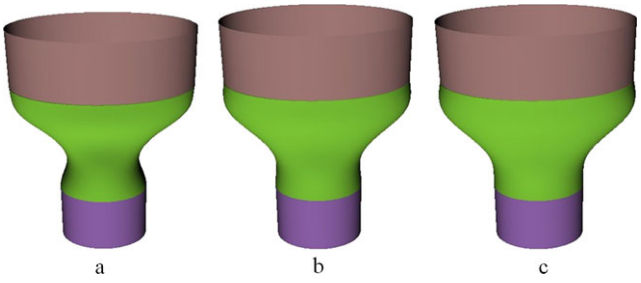

Fig. 6 Effect of the shape control parameter γ on the shape of blending surfaces

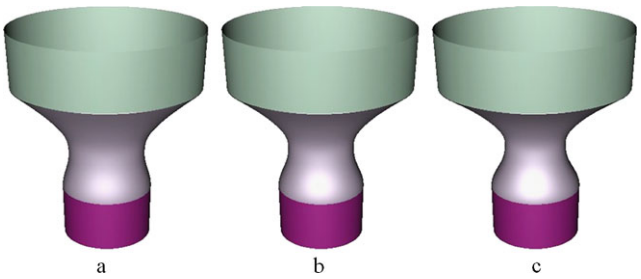

Fig. 7 Effect of the shape control parameter λ on the shape of blending surfaces

How the shape control parameter γ affects the shape of blending surfaces is demonstrated in Fig. 6. The shape control parameters used to create the blending surfaces are: $\beta = \lambda = \rho = 0.01$ and $\eta = -120$. When the shape control parameter γ takes the value of 12, the blending surface in part (a) of the figure is generated. Raising it to 14 and 16, respectively, the blending surfaces in parts (b) and (c) are achieved.

From these images, we can conclude that the shape control parameter γ has a bigger influence on the upper part of blending surfaces. Raising the value of γ from 12 to 16 makes the upper part more convex.

Finally, we examine the impact of the shape control parameter λ on the shape of blending surfaces; see Fig. 7. To this end, the shape control parameters are set to: $\beta = \eta = 0.01$, $\gamma = 10$ and $\rho = 1$. When the shape control parameter λ is set to 60, the blending surface in part (a) of the figure is produced. Increasing it to 80, the shape in part (b) is reached. Further raising it to 100, the blending surface in part (c) is obtained.

The images in Fig. 7 show a strong impact of the shape control parameter λ on the whole blending surface. Increasing it makes the blending surface more concave.

5 Blending applications

In this section, we investigate the applications of the proposed approach in blending different varying parametric surfaces.

For the first application example, the top and bottom primary surfaces change their shapes linearly. They vary from an open surface to a closed one and from a plane to a cone-shaped frustum, respectively.

At the top trimline, the blending boundary constraints for this blending task are:

$$
\begin{aligned}
&u = 0,\\
&S_x(u,v,t) = (1-t)\big[b_1\sinh(a_1v+a_2)\\
&\qquad + b_2\sin(a_3v)\big] + b_3t\cos(-v),\\
&S_y(u,v,t) = (1-t)\big[b_4\cosh(a_4v)\\
&\qquad + b_2\cos(a_3v)\big] + b_5t\sin(-v),\\
&S_z(u,v,t) = (1-t)(h_0+b_5) + h_1t,\\
&\partial S_x(u,v,t)/\partial u = 0.0,\\
&\partial S_y(u,v,t)/\partial u = 0.0,\\
&\partial S_z(u,v,t)/\partial u = -(1-t)b_5.
\end{aligned}
\tag{29}
$$

At the bottom trimline, the blending boundary constraints become:

$$
\begin{aligned}
&u = 1,\\
&S_x(u,v,t) = 0.8(1-t)b_6\sin(a_5v) + b_7t\cos(-v),\\
&S_y(u,v,t) = 0.8(1-t)b_6\cos(a_5v) + b_8t\sin(-v),\\
&S_z(u,v,t) = (1-t)h_3 + h_4t,\\
&\partial S_x(u,v,t)/\partial u = (1-t)b_6\sin(a_5v),\\
&\partial S_y(u,v,t)/\partial u = (1-t)b_6\cos(a_5v),\\
&\partial S_z(u,v,t)/\partial u = -h_5t.
\end{aligned}
\tag{30}
$$

The basic functions for this blending task are: $F_1(v,t)=1$, $F_2(v,t)=t$, $F_3(v,t)=\sin(a_3v)$, $F_4(v,t)=\cos(a_3v)$, $F_5(v,t)=\sin(a_5v)$, $F_6(v,t)=\cos(a_5v)$, $F_7(v,t)=\sinh(a_1v+a_2)$, $F_8(v,t)=\cosh(a_4v)$, $F_9(v,t)=t\sin(-v)$, $F_{10}(v,t)=t\cos(-v)$, $F_{11}(v,t)=t\sin(a_3v)$, $F_{12}(v,t)=t\cos(a_3v)$, $F_{13}(v,t)=t\sin(a_5v)$, $F_{14}(v,t)=t\cos(a_5v)$, $F_{15}(v,t)=t\sinh(a_1v+a_2)$, and $F_{16}(v,t)=t\cosh(a_4v)$.

According to these functions, the known constants are: $b_{x7}=-b_{x15}=b_1$, $b_{x3}=-b_{x11}=b_2$, $b_{x10}=b_3$, $b_{y8}=-b_{y16}=b_4$, $b_{y4}=-b_{y12}=b_2$, $b_{y9}=b_5$, $b_{z1}=h_0+b_5$, $b_{z2}=h_1-(h_0+b_5)$, $\bar{b}_{z1}=-b_5$, $\bar{b}_{z2}=b_5$, $d_{x5}=-d_{x13}=0.8b_6$, $d_{x10}=b_7$, $d_{y6}=-d_{y14}=0.8b_6$, $d_{y9}=b_8$, $d_{z1}=h_3$, $d_{z2}=h_4-h_3$, $\bar{d}_{x5}=-\bar{d}_{x13}=b_6$, $\bar{d}_{y6}=-\bar{d}_{y14}=b_6$, $\bar{d}_{z2}=-h_5$, and all other elements of $\mathbf{b}_j$, $\bar{\mathbf{b}}_j$, $\mathbf{d}_j$ and $\bar{\mathbf{d}}_j$ are zero.

With our proposed approach, the blending surface between the two time-dependent varying primary surfaces is created. In Fig. 8, we give the shapes of the blending surface at the time $t=i/10$ ($i=0,1,2,3,\ldots,10$). The images in the figure indicate that although the two primary surfaces continuously change their shapes, the proposed approach can create a blending surface which smoothly connects these shapes together.

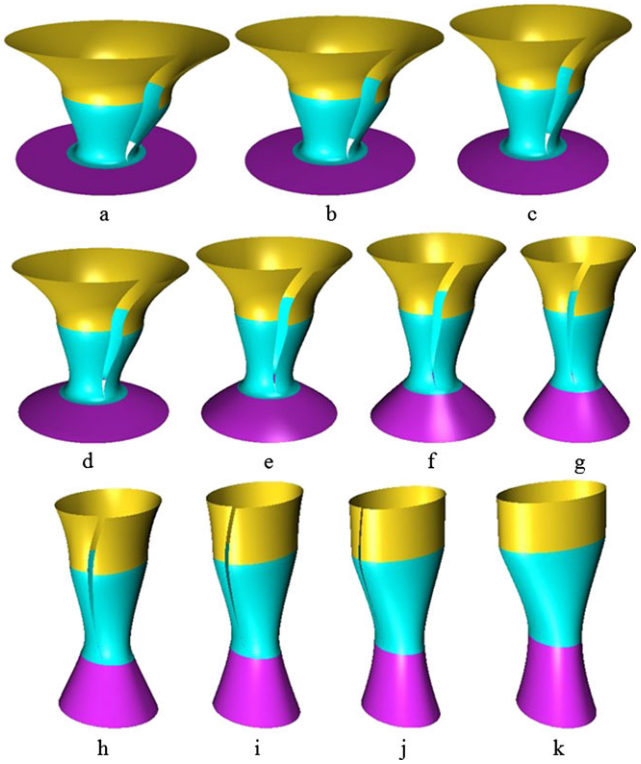

Fig. 8 Blending between two linearly varying primary parametric surfaces

For the second example, two primary surfaces change their shapes following a nonlinear sine variation. The top primary surface initially has some wrinkles, and finally becomes the frustum of a smooth inclined circular cone. The bottom primary surface changes from a cone-shaped elliptic cylinder to an inclined plane.

At the top trimline, the blending boundary constraints for this blending task are:

$$
\begin{aligned}
&u = 0,\\
&S_x(u,v,t) = (1-\sin\pi t/2)(r_0\cos v + r_1\cos kv)\\
&\qquad + 0.36r\sin\pi t/2\cos v,\\
&S_y(u,v,t) = (1-\sin\pi t/2)(r_0\sin v + r_1\sin kv)\\
&\qquad + 0.36r\sin\pi t/2\sin v,\\
&S_z(u,v,t) = (1-\sin\pi t/2)h_0 + \sin\pi t/2(h_{31}\\
&\qquad + 0.6h_{32} + h_{33}\cos v),\\
&\partial S_x(u,v,t)/\partial u = 1.2r\sin\pi t/2\cos v,\\
&\partial S_y(u,v,t)/\partial u = 1.2r\sin\pi t/2\cos v,\\
&\partial S_z(u,v,t)/\partial u = -h_1(1-\sin\pi t/2) + h_{32}\sin\pi t/2.
\end{aligned}
\tag{31}
$$

At the bottom trimline, the blending boundary constraints become:

$$
\begin{aligned}
&u = 1,\\
&S_x(u,v,t) = 1.5(1-\sin\pi t/2)a\cos v\\
&\qquad\qquad + 0.8r_3\sin\pi t/2\cos\alpha\cos v,\\
&S_y(u,v,t) = 1.5(1-\sin\pi t/2)b\sin v + 0.8r_3\sin\pi t/2\sin v,\\
&S_z(u,v,t) = (1-\sin\pi t/2)(h_3 - 0.5h_4)\\
&\qquad\qquad + \sin\pi t/2(h_{41} + 0.8h_{42}\sin\alpha\cos v),\\
&\partial S_x(u,v,t)/\partial u = -(1-\sin\pi t/2)a\cos v\\
&\qquad\qquad + r_3\sin\pi t/2\cos\alpha\cos v,\\
&\partial S_y(u,v,t)/\partial u = -(1-\sin\pi t/2)b\sin v\\
&\qquad\qquad + r_3\sin\pi t/2\cos v,\\
&\partial S_z(u,v,t)/\partial u = -h_4(1-\sin\pi t/2)\\
&\qquad\qquad + h_{42}\sin\pi t/2\sin\alpha\cos v.
\end{aligned}
\tag{32}
$$

Using the proposed method, a blending surface is generated whose shapes at the time $t = i/10$ $(i = 0, 1, 2, 3\ldots, 10)$ are depicted in Fig. 9(a)–(k).

These images also demonstrate the capacity of our proposed approach in smoothly connecting two separate time-dependent varying primary surfaces together.

6 Conclusions

In this paper, we have introduced a new concept of blending time-dependent varying surfaces. Unlike existing surface blending methods which create a static blending surface between two static primary surfaces, the proposed blending method creates a dynamic blending surface between varying parametric surfaces.

When the primary surfaces change from one shape to another, the blending surface also changes its shape accordingly, and the velocity and acceleration will influence the change. Such surface blending is formulated as a boundary-valued dynamic problem.

The shape control parameters involved in the mathematical model have been used to control the shape of the blending surfaces and achieve different shape changes while keeping the exact satisfaction of the C1 continuous blending boundary constraints.

A comparison between different methods indicates that our proposed solution demonstrates high efficiency and accuracy. It can be used to create time-dependent dynamic blending surfaces effectively.

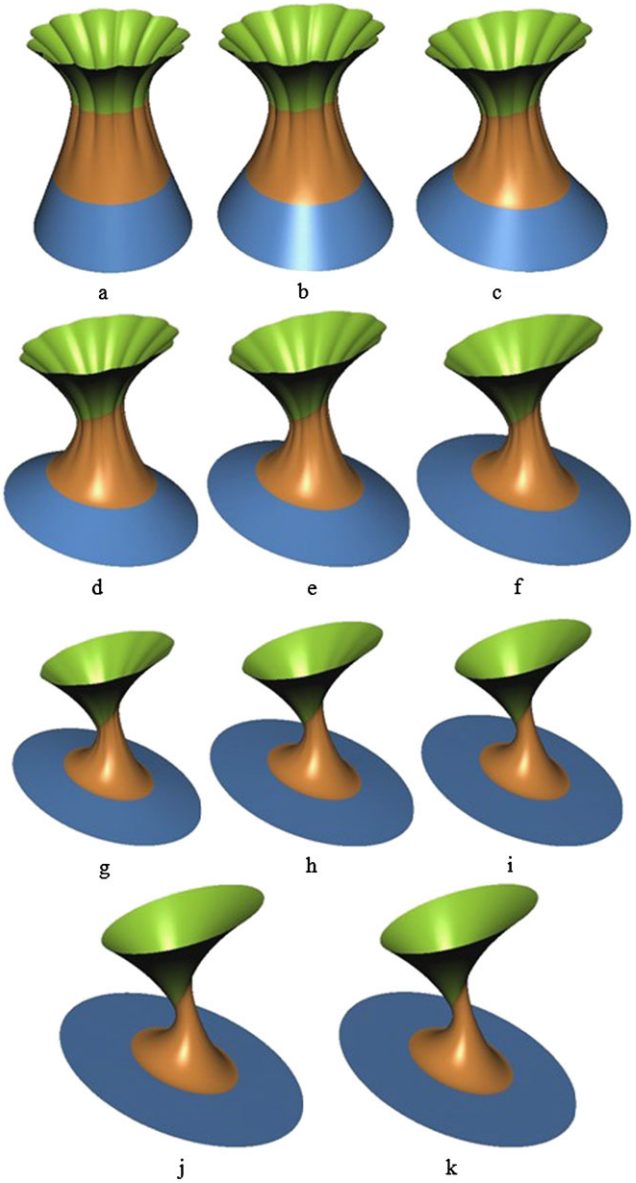

Fig. 9 Blending between two nonlinearly varying primary parametric surfaces

Acknowledgements This research is supported by the grant of UK Royal Society International Joint Projects/NSFC 2010.

References

1. Vida, J., Martin, R.R., Varady, T.: A survey of blending methods that use parametric surfaces. Comput. Aided Des. **26**(5), 341–365 (1994)
2. Rossignac, J.R., Requicha, A.A.G.: Constant-radius blending in solid modeling. CIME, Comput. Mech. Eng. **3**(1), 65–73 (1984)
3. Choi, B.K., Ju, S.Y.: Constant-radius blending in surface modeling. Comput. Aided Des. **21**(4), 213–220 (1989)
4. Sanglikar, M.A., Koparkar, P., Joshi, V.N.: Modelling rolling ball blends for computer aided geometric design. Comput. Aided Geom. Des. **7**, 399–414 (1990)

5. Barnhill, R.E., Farin, G.E., Chen, Q.: Constant-radius blending of parametric surfaces. Computing, Suppl. **8**, 1–20 (1993)
6. Chuang, J.-H., Lin, C.-H., Hwang, W.-C.: Variable-radius blending of parametric surfaces. Vis. Comput. **11**, 513–525 (1995)
7. Farouki, R.A.M., Sverrisson, R.: Approximation of rolling-ball blends for free-form parametric surfaces. Comput. Aided Des. **28**(11), 871–878 (1996)
8. Chuang, J.H., Hwang, W.C.: Variable-radius blending by constrained spine generation. Vis. Comput. **13**, 316–329 (1997)
9. Chuang, J.-H., Lien, P.-L.: One and two-parameter blending for parametric surfaces. J. Inf. Sci. Eng. **14**, 461–477 (1998)
10. Lukács, G.: Differential geometry of G1 variable-radius rolling ball blend surfaces. Comput. Aided Geom. Des. **15**, 585–613 (1998)
11. Kós, G., Martin, R.R., Vrady, T.: Methods to recover constant-radius rolling ball blends in reverse engineering. Comput. Aided Geom. Des. **17**, 127–160 (2000)
12. Bloor, M.I.G., Wilson, M.J.: Generating blend surfaces using partial differential equations. Comput. Aided Des. **21**(3), 165–171 (1989)
13. Cheng, S.Y., Bloor, M.I.G., Saia, A., Wilson, M.J.: Blending between quadric surfaces using partial differential equations. In: Ravani, B. (ed.) Advances in Design Automation, Vol. 1, Computer and Computational Design, pp. 257–263. New York, ASME (1990)
14. Bloor, M.I.G., Wilson, M.J.: Representing PDE surfaces in terms of B-splines. Comput. Aided Des. **22**(6), 324–331 (1990)
15. Bloor, M.I.G., Wilson, M.J.: Using partial differential equations to generate free-form surfaces. Comput. Aided Des. **22**(4), 202–212 (1990)
16. Bloor, M.I.G., Wilson, M.J.: Spectral approximations to PDE surfaces. Comput. Aided Des. **28**(2), 145–152 (1996)
17. Bloor, M.I.G., Wilson, M.J.: Generating blend surfaces using a perturbation method. Math. Comput. Model. **31**(1), 1–13 (2000)
18. Brown, J.M., Bloor, M.I.G., Bloor, M.S., Wilson, M.J.: The accuracy of B-spline finite element approximations to PDE surfaces. Comput. Methods Appl. Mech. Eng. **158**(3–4), 221–234 (1998)
19. Li, Z.C.: Boundary penalty finite element methods for blending surfaces. I. Basic theory. J. Comput. Math. **16**, 457–480 (1998)
20. Li, Z.C.: Boundary penalty finite element methods for blending surfaces. II. Biharmonic equations. J. Comput. Appl. Math. **110**, 155–176 (1999)
21. Li, Z.C., Chang, C.-S.: Boundary penalty finite element methods for blending surfaces. III. Superconvergence and stability and examples. J. Comput. Appl. Math. **110**, 241–270 (1999)
22. You, L.H., Zhang, J.J., Comninos, P.: Blending surface generation using a fast and accurate analytical solution of a fourth order PDE with three shape control parameters. Vis. Comput. **20**, 199–214 (2004)
23. You, L.H., Comninos, P., Zhang, J.J.: PDE blending surfaces with C2 continuity. Comput. Graph. **28**(6), 895–906 (2004)
24. Ugail, H., Bloor, M.I.G., Wilson, M.J.: Techniques for interactive design using the PDE method. ACM Trans. Graph. **18**(2), 195–212 (1999)
25. Zhang, J.J., You, L.H.: Fast surface modeling using a 6th order PDE. Comput. Graph. Forum **23**(3), 311–320 (2004)
26. Gonzalez, C.G., Athanasopoulos, M., Ugail, H.: Cyclic animation using partial differential equations. Vis. Comput. **26**(5), 325–338 (2010)
27. Sheng, Y., Sourin, S., Gonzalez, C.G., Ugail, H.: A PDE method for patchwise approximation of large polygon meshes. Vis. Comput. **26**(6–8), 975–984 (2010)
28. You, L.H., Chang, J., Yang, X., Zhang, J.J.: Solid modeling based on sixth order partial differential equations. Comput. Aided Des. **43**(6), 720–729 (2011)

L.H. You is currently a Senior Research Lecturer at the National Center for Computer Animation, Bournemouth University, UK. He received his M.Sc. degree and Ph.D. degree from Chongqing University, China and another Ph.D. degree from Bournemouth University, UK. His current research interests are in computer graphics, computer animation and geometric modeling. He has produced over 160 refereed publications and is a reviewer for over 30 international journals, some international conferences and funding bodies.

H. Ugail is the director for the Center for Visual Computing at Bradford. He has a first class B.Sc. Honours degree in Mathematics from King's College London and a Ph.D. in the field of Geometric Design from the School of Mathematics at University of Leeds. Prof. Ugail's research interests include geometric modeling, computer animation, functional design, numerical methods and design optimization, applications of geometric modeling to real-time interactive and parametric design and applications of geometric modeling to general engineering problems. Prof. Ugail has 3 patents on novel techniques relating to geometry modeling, animation and 3D data exchange. He is a reviewer for various international journals, conferences and grant awarding bodies. His recent innovations have led to the formation of a university spin-out company Tangentix Ltd. with investments from venture capitalists. He has recently won the Vice-chancellor's Award for Knowledge Transfer for his outstanding contribution to research and knowledge transfer activities.

Jian J. Zhang is currently a Professor of Computer Graphics at the National Center for Computer Animation, Bournemouth University, UK, where he leads the Computer Animation Research Center. He is also a co-founder of the UK Digital Entertainment, which received an initial funding of over six million GBP from the Engineering and Physical Sciences Research Council. His research focuses on a number of topics relating to 3D virtual human modeling, animation and simulation, including geometric modeling, rigging and skinning, motion synthesis, deformation and physics-based simulation.